Atmos. Meas. Tech. Discuss., 6, 11145–11179, 2013
www.atmos-meas-tech-discuss.net/6/11145/2013/
doi:10.5194/amtd-6-11145-2013

Atmospheric Measurement Techniques Discussions

Validation of CM SAF cloud fractions: can cloud cover be reliably derived by satellite data at Hannover, Germany and Lauder, New Zealand? – a comment

A. Werkmeister[1,*], M. Schrempf[1], K. Tohsing[1], M. Lockhoff[2], B. Liley[3], and G. Seckmeyer[1]

[1]Institut für Meteorologie und Klimatologie, Leibniz Universität Hannover, Herrenhäuser Str. 2, 30419 Hannover, Germany
[2]Deutscher Wetterdienst, Frankfurter Str. 135, 63067 Offenbach, Germany
[3]National Institute of Water & Atmospheric Research (NIWA), Lauder, Central Otago, New Zealand
[*]now at: Rosenstiel School of Marine and Atmospheric Science, University of Miami, 4600 Rickenbacker Causeway, FL-33149 Miami, USA

Received: 1 October 2013 – Accepted: 6 December 2013 – Published: 18 December 2013

Correspondence to: G. Seckmeyer (seckmeyer@muk.uni-hannover.de)

Published by Copernicus Publications on behalf of the European Geosciences Union.

Abstract

Cloud Fractional Cover (CFC) derived from Spinning Enhanced Visible and Infrared Imager (SEVIRI) on a geostationary satellite and from the Advanced Very High Resolution Radiometer (AVHRR) on polar orbiters, was validated against ground-based observations in Hannover, Germany (three months of data) and Lauder, New Zealand (only AVHRR, two months of data). The ground-based cloud coverage data consists of synoptical data and imagery taken by a Hemispherical Sky Imager. The standard deviation of the differences between the daily mean CFC derived by SEVIRI and synoptical data was satisfactory, but it was 100 % larger than the deviations of the differences between SEVIRI and those derived by the hemispherical sky imager. For the instantaneous CFC, clear and completely overcast skies are well detected in the satellite products. During broken cloud coverage the agreement between ground-based data from the hemispherical sky imager and data from satellite is mostly uncorrelated. The standard deviations of the differences between AVHRR and the imager (instantaneous and daily mean data) were smaller than those between SEVIRI and imager. In Lauder, New Zealand, only data from the hemispherical sky imager and AVHRR was available. The standard deviations of the differences were slightly higher than in Hannover, Germany. In addition we found that the SEVIRI algorithm systematically overestimates the cloud coverage. We therefore suggest to refine the parameterization of the cloud contamination factor in the algorithms for the derivation of CFC.

1 Introduction

Clouds play an important role in the solar and terrestrial radiation. This consequently leads to an impact on the energy budget and global climate. A small change of cloud parameters may significantly change the temperature variation due to the increase of greenhouse gases (Seinfeld and Pandis, 1998). High clouds, in general, act as

AMTD
6, 11145–11179, 2013

a greenhouse and warm the Earth, whereas low clouds can cool the Earth by reflecting the radiation back to space (Liou, 1991). Furthermore, analysis by Clement et al. (2009) shows observational and model evidence for low-level clouds acting as a positive feedback. They also show that fluctuations in cloud cover appear to be linked to changes in local temperatures and large-scale circulations. This evidence supports the importance of investigating and improving cloud coverage measurements (ground and space based). Also, Solomon et al. (2007) pointed out that the feedback of cloud coverage on the climate is the biggest uncertainty in climate research and forecast.

Several researchers examined the effect of clouds on global and UV radiation enhancements (Calbo et al., 2005; Schafer et al., 2012; Poetzsch-Heffter et al., 1995; Solomon et al., 2007). Clouds can also have an indirect effect on aerosol formation (Forster et al., 2007). Albrecht (1989) explained that increases in aerosol concentrations over the oceans increase the amount of low-level cloudiness. Especially because of their great importance, the understanding of cloud properties, e.g., cloud cover, remains necessary for the weather and climate forecasts.

Though ground observations and measurements often cover longer time scales than satellite based observations, they are not provided in a sufficient spatial coverage.

Only space-based observations can deliver the necessary global coverage with sufficient quality and long time frames. Particularly over the ocean and inaccessible regions satellite data is largely the only data source (Ohring et al., 2005).

The study of clouds has been conducted already in the last decades. The first method of the determination of cloud coverage was human observations. These observations still classify clouds according to the subjective view of shape and appearance by the observer (Robaa, 2008). During the last years more and more of these human-based observations were replaced by ground-based automated instruments to obtain a higher accuracy in cloud coverage estimations (Orsini et al., 2002; Dürr and Philipona, 2004). Dürr and Philipona (2004) developed an Automatic Partial Cloud Amount Detection Algorithm that estimates cloud coverage from surface long-wave downward radiation, surface temperature and relative humidity. Schade

AMTD
6, 11145–11179, 2013

et al. (2009) validated the algorithm by Dürr and Philipona (2004) against human observations and digital all-sky imaging. The results showed that the differences between algorithm and imaging were lower than between algorithm and human cloud estimations. Boers et al. (2010) conducted ground-based measurements based on five different methods that are either passive or active remote sensing instruments. These measurements were compared to a 30 yr climatology of human observations. Their results showed that the observer is mostly underestimating cloud coverage during the day and overestimating at night. Also Martinez-Chico et al. (2011) performed a cloud classification from ground-based instruments. In this case they used radiation data and hemispherical sky images in order to determine different cloud types. They also proposed to use these kinds of studies to determine sites for solar panels to improve the solar resource assessment models. Kazantzidis et al. (2012) compared an automatic estimation of the cloud coverage and classification derived from a simple whole sky imaging system to synoptic data. According to their results, 83 % (broken cloudiness) and 94 % (overcast cloudiness) of the analyzed images agreed within ±1 and ±2 octas compared to the weather observations. They also concluded that the total cloud cover is underestimated when cirrus clouds are present.

Already in the early 1970s, Malberg (1973) compared cloud cover from satellite photographs to ground-based synoptic cloud observations. He explained the differences between ground-based observations and satellite imagery with geometric, synoptic and orographic factors. With increasing availability of satellite data, scientists started developing cloud properties (Ackerman et al., 1998; Christodoulou et al., 2003; Ebert, 1987; Gao and Wiscombe, 1994; Garand, 1988; Parikh, 1977; Porcú and Levizzani, 1992; Romano et al., 2007; Saunders and Kriebel, 1988; Schröder et al., 2002; Welch et al., 1992). The cloud detection threshold tests by Derrien et al. (1993) is a real-time processing scheme that is applied to the different channels of irradiances from the NOAA-11 satellite. This algorithm was further developed and adjusted to new instruments on further satellites (Derrien and LeGleau, 2005, 2013).

AMTD
6, 11145–11179, 2013

The Satellite Application Facility on Climate Monitoring (CM SAF) is part of the European Organization for the Exploitation of Meteorological Satellites – (EUMETSAT) SAF network and generates, archives and distributes satellite-derived products for climate monitoring in an operational mode. CM SAF distributes, among others, cloud products (Cloud Fractional Cover, Cloud Type, Cloud Top Pressure, etc.) derived from the Spinning Enhanced Visible and Infrared Imager (SEVIRI) on the first Meteosat Second Generation geostationary spacecraft and the Advanced Very High Resolution Radiometer (AVHRR) from the polar-orbiting NOAA satellites. These products are directly derived from the physical properties of clouds. The algorithm, which is validated in this work, is NWC SAF PPS 2010 algorithm (Karlsson and Stengel, 2012 which is based on Derrien and LeGleau, 2013 with modifications). The temporal resolutions range from Level 2 instantaneous measurements to Level3 hourly, daily, and monthly averages. The products are available from 1 November 2004 and 1 January 1982 onwards for SEVIRI and AVHRR respectively (further description of CM SAF is given by Schulz et al., 2009 and Woick et al., 2002).

CM SAF published several validation reports in the last years. Deneke et al. (2007) examined comparisons over an eight-month period between MSG/SEVIRI and SYNOP in 2007 with focus on INST, DM and MM. The bias (mean difference) for the INST and DM of each month was approximately 4 % and 12 % respectively, which is consistent with previous work.

Reuter et al. (2009) conducted validation for SEVIRI with synoptic data and initial comparisons with MODIS (Moderate Resolution Imaging Spectrometer) and CALIOP (Cloud–Aerosol Lidar with Orthogonal Polarization). These results showed that the CFC from CM SAF agreed well with synoptic data (within 1 octa difference) and polar orbiting satellite data over midlatitudes. But towards the edges of the visible Earth disk the CFC was overestimated. These results brought them to the conclusion that the clouds might be identified correctly by SEVIRI but are interpreted incorrectly by the algorithm. The horizontal cloud coverage seems larger than in reality just by geometrical viewing effects. The parallax effect results in a displacement of the clouds

AMTD
6, 11145–11179, 2013

positions in relation to the sensor when approaching the edges of foot print. In the same case, not only the position but also the length of these clouds is misinterpreted and the CFC is overestimated.

Amato et al. (2008) performed a statistical analysis of cloud detection from SEVIRI imagery. Their discriminant analysis showed a good performance in cloud detection.

A similar validation has been conducted by Mannstein et al. (2010). Instantaneous comparisons to a Wolkam Camera showed that in a contrail study, the MSG SEVIRI cloud detection algorithm detected 15 % of 79 contrails. These are hard to detect with passive sensors, since they are very thin. The same study was performed with AVHRR, which showed better results due to a higher spatial resolution. The Wolkam Camera in this study confirmed 27 % of the contrails (detailed results in Mannstein et al., 2010).

In this paper, the Cloud Fractional Cover (CFC) products provided by the CM SAF are validated. This means the CFC data are checked in a process of comparisons in order to determine the resilience of the satellite data at instantaneous and daily mean (DM) time scales.

In the next section, the authors will describe the instruments (SEVIRI, AVHRR and HSI), the data retrieval and the data that were used in this work. After introduction of the mathematical methodology, comparisons between the different datasets (SEVIRI, AVHRR, SYNOP and HSI) will be presented. After these comparisons, characteristics of the CFC retrieval algorithm will be investigated. The final section will discuss and conclude the results obtained in this study.

AMTD
6, 11145–11179, 2013

2 Data retrieval and processing

2.1 Data

2.1.1 The Hemispherical Sky Imager (HSI)

The Hemispherical Sky Imager (HSI) was installed on the roof of the Institute of Meteorology and Climatology (IMuK) in Hannover, Germany (52.4° N, 9.7° E). This system is composed of a digital compact charge-coupled device (CCD) camera, a fish-eye objective with a field of view of 183° and a steering unit to provide a hemispherical image of the entire sky. This system is protected by a waterproof enclosure. More details of the HSI system are described in Tohsing et al. (2013). The image acquisition for the cloud coverage determination is performed within 10 s intervals. An identical system is mounted at NIWA (National Institute of Water & Atmospheric Research) in Lauder, New Zealand (45.0° S, 169.7° E. In order to estimate the cloud cover from the HSI image, a camera projection, which describes the relationship between the incoming light ray and the incident angle, needs to be considered. In Tohsing et al. (2013) the camera projection of this camera system has been analyzed and found to be adequate for the cloud cover determination.

The algorithm used in this work for extracting the CFC from Red-Green-Blue (RGB) signal counts is based on the approach by Yamashita et al. (2004). The SkyIndex is defined in order to separate blue sky and cloud areas.

Since the SkyIndex by Yamashita et al. (2004) cannot analyze hemispheric images with an adequate accuracy, the algorithm has been further developed by the Institute of Meteorology and Climatology in Hannover, Germany. In addition to a sun filter, a Haze filter was implemented in the algorithm to analyze uncertain or hazy areas in the digital image by taking into account the green signal counts.

The sun's position in the image is calculated in order to evaluate the mostly bright circular solar area with the sun filter. The HSI, with approximately 3 Mio Pixels, can compute the CFC with a great number of decimals (see Sect. 2).

AMTD
6, 11145–11179, 2013

2.1.2 The SYNOP data

The cloud cover of the SYNOP (surface synoptic observations) data is a numerical code introduced by the World Meteorological Organization. Besides the many meteorological parameters (local temperature, precipitation, visibility etc.) the CFC is delivered every three hours of the day (00:00, 03:00, 06:00, 09:00, 12:00, 15:00, 18:00, and 21:00 UTC). At these times a synoptic observer at a specific location reads the instruments and also estimates several variables, including visibility and CFC. The CFC is reported in octas, ranging from completely clear (zero octas) to completely overcast (eight octas). Since the SYNOP observation takes place about 10 km from the HSI site, it was necessary to analyze whether the two adjacent boxes of the SEVIRI data had equal CFC values. Results showed that during the examined time frame, deviations between the adjacent pixels were always negligible. In conclusion the grid box over the HSI was used.

2.1.3 Radiometers product: Cloud Mask (CMa)

The CMa allows the identification of cloud free areas for remote sensing applications over continental or oceanic surfaces and is a product of the software modules created by the Centre de Meteorologie Spatial (CMS), which takes part in the Satellite Application Facility in supporting NoWCasting and very short range forecasting (NWCSAF). Its main task is to develop and maintain a software package allowing the extraction from MSG/SEVIRI imagery (Derrien and LeGleau, 2005). The cloud detection is performed by a multi-spectral thresholding technique (Derrien and LeGleau, 2005). Version 320 of the CMa-PGE algorithm (Karlsson and Stengel, 2012), which was validated in this work, is a first sequence of tests allowing the identification of pixels contaminated by clouds, snow or ice (Derrien and LeGleau, 2013). If one test is exceedingly successful (i.e. if the threshold is not too close to the measured value) the process is stopped. These tests are applied to land or sea (described in Derrien and LeGleau, 2005) pixels depending on the illumination conditions (daytime, night-time,

AMTD
6, 11145–11179, 2013

etc.) when most thresholds are dynamically determined from satellite-dependent look-up tables and ancillary data. Pixels with measured reflectance and brightness temperatures too close to the threshold are denoted as having low confidence (Derrien and LeGleau, 2005). The tests are detailed in Dybbroe et al. (2005), for SEVIRI and in Derrien and LeGleau (2005) for AVHRR. These tests are robust methods optimizing the use of the rich spectral contents of SEVIRI and AVHRR.

2.1.4 SEVIRI

On board the geostationary satellite MSG (MeteoSat Second Generation) at 36 000 km height above the equator, the SEVIRI provides full disc imagery (at 0° latitude and longitude) over Europe and Africa every 15 min. MSG was launched in 2002 and has been delivering data ever since. The SEVIRI is an optical imaging radiometer with twelve channels (between 0.6 µm and 13.4 µm) and provides unique capabilities for cloud imaging and tracking, fog detection, measurement of the Earth-surface and cloud-top temperatures, tracking of ozone patterns, as well as many other improved measurements. It was constructed by European industry under the leadership of Astrium European Aeronautic Defense and Space Company in Toulouse, France (Aminou, 2002). The twelve SEVIRI channels consist of eight IR detector packages (three detectors each, all made of mercury cadmium telluride), one HRV channel (nine detectors made from indium-doped gallium arsenide), two Visible and one VNIR (three detectors each made from indium-doped gallium arsenide) (Aminou, 2002). SEVIRI has a sampling resolution of 3 km at the nadir in the Infrared channels and a 1 km resolution in the high resolution visible channel (Aminou, 2002).

SEVIRI dataset

Aminou (2002) points out that the Cloud Mask data originally contained 3712 pixel × 3712 pixel and is distributed every 15 min each hour (HH:00, HH:15, HH:30 and HH:45). CM SAF chose a smaller window of the original Cloud Mask of 3636 × 3636

AMTD
6, 11145–11179, 2013

pixels. Transforming this grid to a sinusoidal projection the Cloud Mask is 5925 pixel × 5925 pixel with a resolution of 3 km × 3 km. Averaging the Cloud Mask information over 5 × 5 grid boxes leads to the 1185 × 1185 CFC grid. In accordance with CM SAF processing the CFC was calculated as the fraction of cloudy pixels per sub-region compared to the total number of analyzed pixels per same sub region, which means that the CFC is computed as the cloudy fraction of all pixels within a 15 km × 15 km grid square and is expressed in percent (Karlsson et al., 2009).

2.1.5 AVHRR

The Advanced Very High Resolution Radiometer (AVHRR) is one of the longest satellite observational satellites to date. It operates on board the polar orbiting NOAA satellites (also carried by the Metop-A polar orbiter operated by EUMETSAT since 2006). These measurements began already in the late 1970s and have continued until today (Kogan et al., 2011). The NOAA satellites 15, 16, 18, 19 and Meteorological Operational Satellite (MetOp) –2 belong to the POES (Polar Operational Environmental Satellite) program. These satellites are all equipped with the third version of the AVHRR. The AVHRR is a scanning radiometer, meaning it makes calibrated measurements of upwelling radiation from small areas (scan spots or pixel) which are scanned across the subsatellite track. The operation of the AVHRR is representative of many scanning radiometers on low Earth orbiters (Kidder and Von der Haar, 1995). This scanning radiometer uses 6 detectors that collect different bands of radiation wavelengths between 0.58 µm and 12.50 µm.

AVHRR datasets and similar datasets will be available from sensors on future satellite missions, since these are the instruments which are best suited for climate research. The new instruments will inherit the original AVHRR channels (Karlsson et al., 2013).

AMTD
6, 11145–11179, 2013

AVHRR dataset

The AVHRR dataset has its strengths in the long duration (28 yrs.) and its foundation upon a homogenized AVHRR radiance data record. Quality characteristics are also well investigated and particularly useful results can be found over the tropics, mid- to high-latitudes and over nearly all oceanic areas Karlsson et al. (2013).

Karlsson et al. (2013) introduces a new cloud dataset which is based on AVHRR Global Area Coverage (GAC) data: CLARA-A1. The instantaneous (INST) AVHRR retrievals have a spatial resolution of 1.1 km with pixels spaced at 4.4 km intervals at original swath level.

2.2 Data processing

Both INST satellite datasets (SEVIRI and AVHRR) had to be temporally and/or spatially adjusted in order to be compared to ground-based observations (SYNOP and HSI).

SEVIRI data processing

Since the CM SAF SEVIRI CFC is distributed for HH:45 and the scan by SEVIRI takes twelve minutes (Schmetz et al., 2002) and reaches the area over Hannover after approximately ten minutes, the time HH:00 was chosen for the CFC calculation by HSI and also SYNOP. In order to compare SEVIRI to SYNOP only the values of each third full hour (according to the SYNOP data) have been chosen. A spatial averaging technique is used as well, in order to reconstruct the 1185 × 1185 grid containing the instantaneous CFC.

AVHRR data processing

The HSI data points are chosen according to the overflight time of the polar satellites (NOAA satellites 15, 16, 18, 19 and MetOp-2).

AMTD
6, 11145–11179, 2013

The first step of the algorithm consists in searching these auxiliary data in order to find the right spot of the HSI to which the CFC will be compared. After finding the central pixel (4.5 km × 4.5 km), 3 pixel × 3 pixel (≈ spatial resolution of SEVIRI CFC), each containing information about the cloud situation, are averaged. The result is a 13.5 km × 13.5 km box containing the CFC in %.

3 Methodology

In order to validate and compare the different datasets, statistic relations have been used. The results of this work are based on the following equations from Hartung (1999):

The Daily Mean (DM) is defined by

$$\mathrm{DM} = \frac{1}{k}\sum_{n=1}^{k}\mathrm{CFC}(n), \tag{1}$$

where k is the number of CFC values in one day.

The MAD here is defined as the mean of the absolute differences. The equation becomes:

$$\mathrm{MAD} = \frac{1}{j}\sum_{m=1}^{j}|x_m| \tag{2}$$

where j equals the number of differences between the datasets and x_m is the difference between two datasets.

The standard deviation (StD) is defined by

$$\mathrm{StD} = \sqrt{\frac{1}{l}\sum_{n=1}^{l}(x_n-\mu)^2} \tag{3}$$

AMTD
6, 11145–11179, 2013

where x_n is the difference between two datasets, I is the number of available values and $\mu = \frac{1}{I}\sum_{n=1}^{I} x_n$ is the mean of these differences.

The correlation coefficient Kor(c,a) is defined by

$$\mathrm{Kor}(a,c) = \frac{\sum_{i=1}^{N}(c_i - \overline{c})(a_i - \overline{a})}{\sqrt{\sum_{i=1}^{N}(c_i - \overline{c})^2 \cdot \sum_{i=1}^{N}(a_i - \overline{a})^2}}, \quad (4)$$

where c_i are the values of CFC by SEVIRI, a_i are the values of CFC by the HSI and $\overline{c}, \overline{a}$ are the arithmetical means of the CFC by the respective instrument.

The probability of detection (POD) is based on contingency tables, which indicate the discrete joint distribution:

$$\mathrm{POD} = \frac{\#\text{of differences} = 0}{\text{total \#of observations}}. \quad (5)$$

The false alarm rate (FAC) is a measure of observation performance (just as POD) indicating the ratio between differences $\neq 0$ and total observations:

$$\mathrm{FAC} = \frac{\#\text{of differences} \neq 0}{\text{total \#of observations}}. \quad (6)$$

4 Results

4.1 Comparisons of CFC from satellite and HSI

4.1.1 MSG SEVIRI

Analysis of the relation between the INST CFC of the HSI and SEVIRI for the months July through September 2009 showed the highest number of occurrences when both SEVIRI and HSI have a CFC of zero octas or eight octas (100 %) as shown in Fig. 1.

AMTD
6, 11145–11179, 2013

Fast moving clouds and changing weather also influence the order of the deviations. On 30 July 2009, we recorded fast changing weather conditions. This data is shown in Fig. 2. The three HSI images on the top indicate the present cloud situation at specific times (11:00, 15:50 and 16:00 UTC). The CFC by SEVIRI and HSI is displayed in the plot underneath. HSI captures even small changes in the cloud coverage, whereas SEVIRI, due to its coarser resolution, is unable to detect the same changes in CFC.

The occurrences in Fig. 1 also point out that the number of times when SEVIRI detects a CFC of eight octas (100 %), the HSI has a CFC between two and seven octas. The FAC of these cases is 29 %, whereas the POD is 71 %. Due to Off-nadir effects and different spatial resolutions of the instruments SEVIRI often overestimates the CFC (Martin, 2004). The StD of the two data sets is 2.0 octas or 25 %. The MAD of these two datasets is 1.75 octas (18 %) (results summarized in Table 2).

In conclusion, the results of the INST CFC from SEVIRI show almost one fifth deviation from the HSI due to the lack of high spatial resolution of SEVIRI. Nevertheless, the DM results in a smaller StD of 15 % and a MAD equal to 12 %.

4.1.2 NOAA AVHRR

For the comparison of the CFC from NOAA AVHRR and HSI in Hannover, the CFC has been calculated as described in Sect. 2.2. The computed INST NOAA CFC has varying overflight times. On average, 20 values of CFC are computed for each day, for the box centered in Hannover, Germany. Only the NOAA and HSI CFC with a solar zenith angle lower than 80 are chosen for validation. These are approximately ten values for each dataset per day.

Figure 3 displays the number of occurrences of the INST differences of CFC in octas from both satellite instruments, SEVIRI and AVHRR, to the HSI. The number of occurrences for CFC differences between AVHRR and HSI equaling zero octa (approximately 300) is more than three times larger than the differences of one octa and higher (less than 100). The POD for AVHRR differences is 81 % with a StD of 22 %. This means that in this case, only 20 % of the measurements lies outside the

AMTD
6, 11145–11179, 2013

StD. The numbers of occurrences decrease with higher differences. Since the numbers of occurrences are equally distributed for positive and negative differences, we can conclude that the differences are unbiased (mean difference is almost 0).

The direct comparison to the INST one hour results of SEVIRI leads to the conclusion that the off-nadir effects influence the results of SEVIRI. Originating from polar orbiters, the AVHRR measurements have the advantage that the instrument's nadir passes the desired location at some point, decreasing the off-nadir effect. Another factor contributing to the lower deviations of the AVHRR to the HSI is the original higher resolution of 1 km × 1 km of the AVHRR in comparison to SEVIRI with a resolution of 3 km × 3 km. This leads to better results in the comparisons between AVHRR and HSI compared to the results between SEVIRI and HSI. This statement is supported by the StD of the difference between the CFC of AVHRR and HSI is 22 % (1.8 octas). The MAD is 15 % (1.2 octas) which is over 3 % lower than the results from SEVIRI. A comparison of the DMs for 1 July 2009 through 30 September 2009 of the CFC differences between AVHRR and HSI, and between SEVIRI and HSI respectively, shows that AVHRR – HSI DM CFC and SEVIRI – HSI DM CFC have almost the same maxima and minima on the same days (figure not shown here). The differences of AVHRR – HSI DM CFC are generally smaller in July and larger in September, than the differences from SEVIRI – HSI DM CFC. The StD of the difference for the DM CFC derived from the AVHRR is 14 % (1.15 with a CFC in octas) and the MAD is 12 % (0.94 octas).

The same comparisons have been made for the grid cell over Lauder, New Zealand. For the evaluation of CFC by the AVHRR, the time frame had to be adjusted to the Southern Hemisphere summer in order to acquire enough data by the HSI, which cannot perform a computation of CFC at night. The chosen time frame is 1 November 2009 through 31 December 2009 for which the CFC has been calculated as described in Sect. 2.1.1.

The occurrences of the differences between INST CFC in octas from AVHRR and HSI for November and December 2009 in Lauder, New Zealand in Fig. 3 point out

AMTD
6, 11145–11179, 2013

a high number of accordance when both AVHRR and HSI state a CFC of eight octas (100 %). The occurrences also show that the HSI computes a CFC of one octa, whereas the AVHRR sees a CFC between one and eight octas. This leads to a StD of the instantaneous differences of 2.20 octas (28 %) and a MAD of 1.48 octas (19 %). These differences are slightly larger than those obtained for Hannover, Germany which may also be caused by the shorter time frame. Only two months have been used in the Lauder examinations, whereas the time frame for Hannover was three months. This choice of time frames is due to the fact that the CLARA-A1 data set has only been computed until 31 December 2009.

The difference between DM CFC in % of the AVHRR and HSI for 1 November 2009 through 31 December 2009 in Lauder, New Zealand states a maximum deviation of approximately ±30 % at the beginning of November and the end of December as shown in Fig. 5. During the first two weeks it seems that the AVHRR is either under- or overestimating the CFC compared to the HSI. On the other hand during the last week of November and the entire month of December, the AVHRR underestimates the CFC compared to the HSI. With a StD between the CFC of AVHRR and HSI of 15 % (1.16 octas) and a MAD of 12 % (0.97 octas), the differences are slightly larger than those obtained for Hannover, Germany. The results of both SEVIRI and AVHRR comparisons in Hannover, Germany and Lauder, New Zealand are presented in Table 1.

4.2 Comparisons of Satellite and SYNOP CFC

For the comparison of CFC of SEVIRI and SYNOP in Hannover – Langenhagen, the reconstructed algorithm of the CM SAF, as described in Sect. 2.2, has been used to calculate an INST CFC with a temporal resolution of one hour for SEVIRI data.

Comparisons between the INST CFC datasets of SEVIRI and SYNOP show a StD of the CFC difference of 41 % (3.3 octas) (also shown in Table 2). SYNOP data do not show any moment of clear sky when SEVIRI measures a CFC at 0 %. One has to keep in mind that weather observers only state a CFC with zero octa when there is no sign

AMTD
6, 11145–11179, 2013

of clouds at all (not even at the horizon). When the observer estimates a CFC of zero octa SEVIRI mostly estimates a CFC between six and eight octas.

The MAD is found to be 51 % (4.1 octas).

Compared to the results of SEVIRI – HSI, the SYNOP data shows a higher amount of numbers of deviations (see Fig. 4). The histogram displays the number of occurrences of the difference between CFC in octas from SEVIRI to both HSI and SYNOP. In order to compare both datasets to the SYNOP data the occurrence of differences has been adjusted to the number of data points of the SYNOP. The differences with the HSI show a peak at a difference of zero octa with the occurrence of about 140 counts, whereas the differences with the SYNOP data have a peak at one octa, indicating an underestimation by SYNOP, with an occurrence of 70 counts. The probability of detection (POD) between SYNOP and SEVIRI is 43 %, which points out that statistically, every second measurement lies out of the range of the StD. Accordingly, the FAC is 56 %. We can also determine that both differences show a higher number of occurrences for the positive differences than for the negative differences, concluding an overestimated CFC by SEVIRI. The differences of the DM CFC from SEVIRI to SYNOP show higher results (up to 100 %), than the differences of SEVIRI – to HSI especially in the month of September 2009. The StD of the difference between SEVIRI – SYNOP is 32 %, whereas the StD of the difference between SEVIRI – HSI is 15 %. The MAD is at 12 % and 25 % for HSI and SYNOP respectively as shown in Table 2.

4.3 SEVIRI algorithm adjustments

Detailed analyses were conducted in order to examine the influence of different adjustments (e.g., grid size, CCF) by the CM SAF algorithm on the results of the CFC. For this validation of the CFC product (in one hour matchups), the original adjustments were used to examine the original product, which is currently published by CM SAF.

AMTD
6, 11145–11179, 2013

4.3.1 Variation of cloud contamination factor

In the CMa file each pixel provides information about the cloud situation. One item is the cloud contamination, which is originally assigned the value of 100 % by CM SAF. Since the pixel is not completely cloud filled, a CFC of 100 % is not the correct assigned value. Hence, there was a need to examine whether a Cloud Contamination Factor (CCF) of 100 % is the best choice. In the following analyses the CCF is varied between 50 %, 75 %, and 100 % for the CFC calculation and the resulting CFC is then compared to the CFC of the HSI.

A CCF of 75 % is the best-fitting dataset for instantaneous temporal resolution. This is based on the StDs and mean of all different absolute differences between SEVIRI (with the varied CCFs) and HSI data. The lowest StD is 22 % and the MAD is 16 %. Combining the analysis of different CFC and different Cloud Contamination Factors, the results reveal that with the same CCF and various grid sizes, the deviations are nearly identical and have the same behavior. The results of the difference between SEVIRI with a CCF of 100 % and HSI point out consistently the highest values, while the graphs with a CCF of 50 % show consistently the lowest values. The SEVIRI CFC with a grid size of 3 pixel × 3 pixel and a CCF of 75 % has the lowest results in StD and MAD. Here the StD is 14 %. On the other hand, the CFC derived from a 7 pixel × 7 pixel and 100 % CCF has the lowest MAD of 12 %.

In conclusion, a Cloud Contamination Function, which varies between 75 % and 100 % can carry the best fit for INST, DM and MM data. Indeed, the results show a lower mean of the absolute differences for any grid number for a CCF of 100 %, and the lowest StD for any grid size is always obtained by a CCF of 75 %. In addition the average over 7 pixel × 7 pixel show the best results for instantaneous comparisons and is in conclusion the best fit.

AMTD
6, 11145–11179, 2013

4.3.2 CFC distribution

To determine the importance of the days that were not clear sky or covered sky days, we distinguished between the number of occurrences for each CFC of zero and eight octas, and the number of occurrences for CFC between one and seven octas. The days of agreement between satellite and HSI are days when no clouds occur or the sky is fully covered. These days have a StD lower than 10 %. All other days show StDs between 20 and 48 %.

The empirical correlation coefficient Kor(c, a) (Eq. 4) has been calculated for the days with StDs greater than ten and for days with StDs lower than 10 %. The correlation coefficient for days with StDs less than 10 % is 0.9, which means that 81 % of the CFC distribution of SEVIRI can be explained by the CFC of the HSI. This result indicates that the correlation is high enough to state a correlation between SEVIRI and HSI CFC for completely overcast or clear days. Both SEVIRI and HSI show almost the same high number of occurrences for a CFC at eight octas.

The correlation coefficient for days with StDs higher than 10 % is 0.6, indicating that only 36 % of the CFC distribution of SEVIRI can be explained by the CFC of the HSI. This means that the correlation in this case is not significant enough and that the CFC of SEVIRI and HSI does not correlate. For these days, the occurrences of zero and eight octas of SEVIRI CFC are very high. The occurrences of the HSI CFC are almost equally distributed between two and seven octas with a maximum number of occurrences at eight octas. The number of occurrences of CFC > 0 % by HSI is not as high as the number of occurrences of CFC by SEVIRI. These disagreements are due to the CFC algorithm, more specifically due to the CCF. If the sky is neither clear nor fully clouded, a cloud contaminated pixel occurs, and is assigned the value of 100 %. If a cloud contaminated pixel is in reality only 10 % filled, it is assigned a factor of 100 % (constant CCF). This leads to a false CFC and to a non-correlating CFC by HSI and SEVIRI.

AMTD
6, 11145–11179, 2013

5 Conclusions and discussions

5.1 Evaluation of satellite CFC with SYNOP data

INST and DM cloud fractional cover from SEVIRI and SYNOP data were compared. INST often shows a high deviation of 100 % between SEVIRI data and SYNOP data for Hannover. The POD of SEVIRI and SYNOP is 44 %. The comparison of DM CFC shows that the StD between both datasets is about 32 %. A factor that is contributing to the deviations between SYNOP and SEVIRI CFC is the subjective estimation by different weather observers who are working in shifts. Therefore, these estimations depend on the physical conditions of human beings. Even trained observers tend to over- or underestimate cloud coverage (Dybbroe et al., 2004). Another factor influencing these validations is the area that is considered by the observer, which is highly dependent on the present visibility. These influences contribute to the conclusion that synoptic observations of CFC are less suited for instantaneous validation of instrument based SEVIRI CFC than continuous stable machine operated measurements.

5.2 Evaluation of Satellite CFC with HSI data

The validation of the CFC from SEVIRI with HSI data showed up to 100 % variation of the INST. For completely cloudy skies the SEVIRI and HSI estimate the same CFC. For clear sky days the SEVIRI shows no amount of clouds, whereas the HSI still notices a CFC of up to 5 % due to the solar filter, which does not exclude the sun entirely. The DM results showed deviations of up to 40 % between the two datasets, whereas the mean of absolute differences is only 12 %. This also means that, statistically, in 33 % of all cases the deviations are higher than 12 % with the assumption of a Gaussian distribution. In conclusion we can say that in the case of broken cloud fields (2–6 octas) the INST CFC should be treated with caution. Whereas the averaged climatology may well be used for validation against ground-based observations. In addition, INST and

AMTD
6, 11145–11179, 2013

DM CFC from HSI were compared to AVHRR NOAA satellite data. The AVHRR shows nearly the same deviations as SEVIRI with slightly smaller magnitude in INST and DM, which means that both instruments are sensitive to the same weather conditions (convective clouds, high winds and fast changing weather conditions) as shown in the results of New Zealand. Humidity in the upper atmosphere is a cause, which leads to an incorrect interpretation of the cloud situation by the HSI. Some cirrus clouds are too thin to be detected in the visible spectrum. Another cause is the spatial resolution, limits and form of one box by the AVHRR, which differs from the field of view and form of the HSI.

The influence of the different cloud contamination factors for the CFC was also analyzed. The cloud contamination factor of 50 %, 75 % and 100 % had been applied to determine the CFC from SEVIRI data. Subsequently this CFC had been compared with the cloud fractional cover from the HSI. The results show that the best correspondence in INST, DM and MM is between the CFC of SEVIRI and HSI data for cloud contamination values between 75–100 %, which agrees with the results obtained by Deneke et al. (2007). Further evaluations of the CFC distribution showed higher deviations between ground and satellite measurements when choosing a constant CCF. Atmospheric factors which should be considered when choosing the CCF, are for example, partly clouded skies. One deficiency contributing to the INST and in conclusion to the DM deviation of the CFCs, is the circumsolar area of the sun that is not perfectly analyzed by the sun filter in the HSI algorithm. As a result, this bright area is incorrectly characterized as cloud contaminated or filled leading to an error up to 5 %. Another effect contributing is the occurrence of stratocumulus. These clouds have small areas where blue sky is exposed, which are detected by the HSI. Because of the small scale and only slight transparency of these areas, they are assigned a wrong CCF of a 100 %. This is causing a higher computed CFC. A third effect contributing to the deviations are less readily detectable cirrus clouds. These clouds are either not detected by the HSI because of their high transparency for the blue portion of the spectrum of the sky radiance or are not detected by the satellite instrument because of

AMTD
6, 11145–11179, 2013

the lack of cloud particles per volume of the cloud. We recommend introducing a cloud coefficient function which varies according to the measurements.

The distribution of the cloud fractional cover of the days with a StD lower and higher than 10 % has been examined, in order to determine the uncertainty contributing to the deviations between the cloud fractional cover from HSI and SEVIRI data. From the correlation coefficient and the cloud fractional cover for both cases, one can conclude that the CFC algorithm (influenced by spatial resolution and vision effects) is not accurate enough for days with a StD higher than 10 %. These days especially consist of CFCs between zero and seven octas. Despite the influences of instrument characteristics (swath width, height, spatial resolution), pixels which are interpreted as cloud contaminated are assigned a constant 100 % CCF and not a variable CCF. This constant CCF decreases the correlation coefficient to 0.6 compared to 0.9 of days with a StD lower than 10 % (consisting of mostly CFCs of eight octas).

Although instantaneous measurements are not as reliable as ground-based measurements, which have a higher spatial resolution, satellite based datasets are very valuable for applications/studies ranging from small spatial scales and short temporal resolution over seasonal to multi-annual scales. However, validation with ground-based data must be an integral part of all satellite programs. For such validation programs we recommend a more frequent use of ground-based equipment like cloud cameras to improve further validations and developments of satellite data, algorithms and instrumentations.

Acknowledgements. The authors gratefully thank NIWA staff Michael Kotkamp, Richard McKenzie for keeping the cloud camera running at Lauder, New Zealand. We thank EUMETSAT's Satellite Application Facility on Climate Monitoring (CM SAF) for providing the data that has been used in this work. We acknowledge support by Deutsche Forschungsgemeinschaft and Open Access Publishing Fund of Leibniz Universität Hannover.

AMTD
6, 11145–11179, 2013

References

Ackerman, S. A., Strabala, K. I., Menzel, W. P., Frey, R. A., Moeller, C. C., and Gumley, L. E.: Discriminating clear sky from clouds with MODIS, J. Geophys. Res.-Atmos., 103, 32141–32157, 1998. 11148

Albrecht, B. A.: Aerosols, cloud microphysics, and fractional cloudiness, Science, 245, 1227–1230, 1989. 11147

Amato, U., Antoniadis, A., Cuomo, V., Cutillo, L., Franzese, M., Murino, L., and Serio, C.: Statistical cloud detection from SEVIRI multispectral images, Remote Sens. Environ., 112, 750–766, 2008. 11150

Aminou, D.: MSG's SEVIRI Instrument, ESA Bull.-Eur. Space, 111, 15–17, 2002. 11153

Boers, R., de Haij, M., Wauben, W., Baltink, H. K., van Ulft, L., Savenije, M., and Long, C. N.: Optimized fractional cloudiness determination from five ground-based remote sensing techniques, J. Geophys. Res.-Atmos., 115, D24116, 2010. 11148

Calbo, J., Pages, D., and Gonzales, J.: Empirical studies of cloud effects on UV radiation: a review, Rev. Geophys., 43, 1–28, 2005. 11147

Christodoulou, C. I., Michaelides, S. C., and Pattichis, C. S.: Multifeature texture analysis for the classification of clouds in satellite imagery, IEEE T. Geosci. Remote, 41, 2662–2668, 2003. 11148

Clement, A. C., Burgman, R., and Norris, J. R.: Observational and model evidence of positive low-level cloud feedback, Science, 325, 460–464, 2009. 11147

Deneke, H., Johnston, S., Reuter, M., Roebeling, R., Tetlaff, A., Thomas, W., and Wolters, E.: Validation of CM SAF Cloud Products Derived from MSG/SEVIRI Data, Tech. rep., CM SAF Deutscher Wetterdienst, 2007. 11149, 11165

Derrien, M. and LeGleau, H.: MSG/SEVIRI Cloud Mask and Type from SAFNWC, Int. J. Remote Sens., 26, 4707–4732, 2005. 11148, 11152, 11153

Derrien, M. and LeGleau, H.: Algorithm theoretical basis document for cloud products, Tech. rep., NWCSAF, 2013. 11148, 11149, 11152

Derrien, M., Farki, B., Harang, L., LeGleau, H., Noyalet, A., Pochic, D., and Sairouni, A.: Automatic cloud detection applied to NOAA-11/AVHRR imagery, Remote Sens. Environ., 46, 246–267, 1993. 11148

Dürr, B. and Philipona, R.: Automatic cloud amount detection by surface longwave downward radiation measurements, J. Geophys. Res.-Atmos., 109, 1–9, 2004. 11147, 11148

AMTD
6, 11145–11179, 2013

Dybbroe, A., Karlsson, K. G., and Thoss, A.: NWCSAF AVHRR cloud detection and analysis using dynamic thresholds and radiative transfer modeling, Part II: Tuning and validation, J. Appl. Meteorol., 44, 55–71, 2004. 11164

Dybbroe, A., Thoss, A., and Karlsson, K.-G.: NWCSAF AVHRR cloud detection and analysis using dynamic thresholds and radiative transfer modeling, Part I: Algorithm description, J. Appl. Meteorol., 44, 39–54, 2005. 11153

Ebert, E.: A pattern recognition technique for distinguishing surface and cloud types in the polar regions, J. Clim. Appl. Meteorol., 26, 1412–1427, 1987. 11148

Forster, P., Ramaswamy, V., Artaxo, P., Berntsen, T., Betts, R., Fahey, D., Haywood, J., Lean, J., Lowe, D., Myhre, G., Prinn, R., Raga, G., Schultz, M., and VanDorland, R.: Changes in Atmospheric Constituent and in Radiative Forcing, Tech. rep., United States Environmental Protection Agency, 2007. 11147

Gao, B.-C., and Wiscombe, W.: Surface-Induced Brightness Temperature Variations and Their Effects on Detecting Thin Cirrus Clouds Using IR Emission Channels in the 8–12 micron Region., J. Appl. Meteorol., 33, 568–572, 1994. 11148

Garand, L.: Automated recognition of oceanic cloud patterns, Part I: Methodology and application to cloud climatology, J. Climate, 1, 20–39, 1988. 11148

Hartung, J.: Statistik, Oldenbourg Verlag, 1999. 11156

Karlsson, K. G. and Stengel, M.: CM SAF Cloud, Albedo, Radiation dataset, AVHRR-based, Edition 1 (CLARA-A1): Cloud Products – Algorithm Theoretical Basis Document, Tech. rep., CM SAF Deutscher Wetterdienst, 2012. 11149, 11152

Karlsson, K.-G., Lockhoff, M., A. Devasthale, A., and Dybbroe, A.: Validation of CM – SAF Cloud Products Derived from AVHRR Data in the Arctic Region, Tech. rep., CM – SAF Deutscher Wetterdienst, 2009. 11154

Karlsson, K.-G., Riihelä, A., Müller, R., Meirink, J. F., Sedlar, J., Stengel, M., Lockhoff, M., Trentmann, J., Kaspar, F., Hollmann, R., and Wolters, E.: CLARA-A1: a cloud, albedo, and radiation dataset from 28 yr of global AVHRR data, Atmos. Chem. Phys., 13, 5351–5367, doi:10.5194/acp-13-5351-2013, 2013. 11154, 11155

Kazantzidis, A., Tzoumanikas, P., Bais, A., Fotopoulos, S., and Economou, G.: Cloud detection and classification with the use of whole-sky ground-based images, Atmos. Res., 113, 80–88, 2012. 11148

Kidder, S. and von der Haar, T.: Satellite Meteorology an Introduction, Academic Press, San Diego, 1995. 11154

AMTD
6, 11145–11179, 2013

Kogan, F., Vargas, M., and Guo, W.: Comparisonof AVHRR-Based Global Data Records, in Use of Satellite and In-Situ Data to Improve Saustainability, Springer Science+Business, 2011. 11154
Liou, K.: Encyclopedia of Earth Systems; Atmospheric radiation: Causes and Effects, Academic Press, 1991. 11147
Malberg, H.: Comparison of mean cloud cover obtained by satellite photographs and ground-based observations over Europe and the Atlantic, Mon. Weather Rev., 101, 893–897, 1973. 11148
Mannstein, H., Brömser, A., and Bugliaro, L.: Ground-based observations for the validation of contrails and cirrus detection in satellite imagery, Atmos. Meas. Tech., 3, 655–669, doi:10.5194/amt-3-655-2010, 2010. 11150
Martin, S.: An Introduction to Ocean Remote Sensing, Cambridge University Press, 2004. 11158
Martinez-Chico, M., Batlles, F., and Bosch, J.: Cloud classification in a mediterranean location using radiation data and sky images, Energy, 36, 4055–4062, 2011. 11148
Ohring, G., Wielicki, B., Spencer, R., Emery, B., and Datla, R.: Satellite instrument calibration for measuring global climate change, B. Am. Meteorol. Soc., 86, 1303–1313, 2005. 11147
Orsini, A., Tomasi, C., Calzolari, F., Nardino, M., Cacciari, A., and Georgiadis, T.: Cloud cover classification through simultaneous ground-based measurements of solar and infrared radiation, Atmos. Res., 61, 251–275, 2002. 11147
Parikh, J.: A comparative study of cloud classification techniques, Remote Sens. Environ., 6, 67–81, 1977. 11148
Poetzsch-Heffter, C., Liu, Q., Ruperecht, E., and Simmer, C.: Effect of cloud types on the earth radiation budget calculated with the ISCCP C1 dataset: methodology and initial results, J. Climate, 8, 829–843, 1995. 11147
Porcú, F. and Levizzani, V.: Cloud classification using METEOSAT VIS-IR imagery, Int. J. Remote Sens., 13, 893–909, 1992. 11148
Reuter, M., Thomas, W., Albert, P., Lockhoff, M., and Weber, R.: The CM SAF and FUB cloud detection schemes for SEVIRI: validation with synoptic data and initial comparison with MODIS and CALIPSO, J. Appl. Meteorol. Clim., 48, 301–316, 2009. 11149
Robaa, S.: Evaluation of sunshine duration from cloud data in Egypt, Energy, 33, 785–795, 2008. 11147

AMTD
6, 11145–11179, 2013

Romano, F., Cimini, D., Rizzi, R., and Cuomo, V.: Multilayered cloud parameters retrievals from combined infrared and microwave satellite observations, J. Geophys. Res., 112, D08210, doi:10.1029/2006JD007745, 2007. 11148

Saunders, R. and Kriebel, K.: An improved method for detecting clear sky and cloudy radiances from AVHRR data, Int. J. Remote Sens., 9, 123–150, 1988. 11148

Schade, N. H., Macke, A., Sandmann, H., and Stick, C.: Total and partial cloud amount detection during summer 2005 at Westerland (Sylt, Germany), Atmos. Chem. Phys., 9, 1143–1150, doi:10.5194/acp-9-1143-2009, 2009. 11147

Schafer, J., Saxena, V., Wenny, B., Barnard, W., and DeLuisi, J.: Observed Influence of Clouds on Ultraviolet-B Radiation, Geophys. Res. Lett., 23, 2625–2628, 2012. 11147

Schmetz, J., Pili, P., Tjemkes, S., Just, D., Kerkmann, J., Rota, S., and Ratier, A.: An Introduction to Meteosat Second Generation (MSG), American Meteorological Society, 83, 977–992, 2002. 11155

Schröder, M., Bennartz, R., Schüller, L., Preusker, R., Albert, P., and Fischer, J.: Generating cloudmasks in spatial high-resolution observations of clouds using texture and radiance information, Int. J. Remote Sens., 23, 4247–4261, 2002. 11148

Schulz, J., Albert, P., Behr, H.-D., Caprion, D., Deneke, H., Dewitte, S., Dürr, B., Fuchs, P., Gratzki, A., Hechler, P., Hollmann, R., Johnston, S., Karlsson, K.-G., Manninen, T., Müller, R., Reuter, M., Riihelä, A., Roebeling, R., Selbach, N., Tetzlaff, A., Thomas, W., Werscheck, M., Wolters, E., and Zelenka, A.: Operational climate monitoring from space: the EUMETSAT Satellite Application Facility on Climate Monitoring (CM-SAF), Atmos. Chem. Phys., 9, 1687–1709, doi:10.5194/acp-9-1687-2009, 2009. 11149

Seinfeld, J. and Pandis, S.: Atmospere Chemistry and Physics: From Air Pollution to Climate Change, Wiley & Sons, New York, 1998. 11146

Solomon, S., Qun, D., Manning, M., Chen, Z., Marquis, M., Averyt, K. B., Tignor, M., and Miller, H. L. (Eds.): Climate Change 2007: the Physical Science Basis: Contribution of Worki Group I to the Forth Assessment Report of the Intergovernmental Panel of Climate Change, Cambridge University Press, 2007. 11147

Tohsing, K., Schrempf, M., Riechelmann, S., Schilke, H., and Seckmeyer, G.: Measuring High-Resolution Sky Luminance Distributions with a CCD Camera, Appl. Optics, 52, 1564–1573, 2013. 11151

AMTD
6, 11145–11179, 2013

Welch, R., Sengupta, S., Goroch, A., Rabindra, P., Rangaraj, N., and Navar, M.: Polar cloud and surface classification using AVHRR imagery: an intercomparison of methods, J. Appl. Meteorol., 31, 405–420, 1992. 11148

Woick, H., Dewitte, S., Feijt, A., Gratzki, A., Hechler, P., Hollmann, R., Karlsson, K. G., Laine, V., Loewe, P., Nitsche, H., Werscheck, M., and Wollenweber, G.: The Satellite Application Facility on Climate Monitoring, Adv. Space Res., 30, 2405–2410, 2002. 11149

Yamashita, M., Yoshimura, M., and Nakashizuka, T.: Cloud Cover Estimation Using Multitemporal Hemisphere Imageries, International Archives of Photogrammetry, Remote Sensing and Spatial Information, 35, 826–829, 2004. 11151

AMTD
6, 11145–11179, 2013

Table 1. Results of the validation of the instantaneous and daily SEVIRI and AVHRR data in Hannover (H.), Germany and AVHRR data in Lauder (L.), New Zealand. The data has been compared to the HSI and the results are presented as StD, MAD, POD and FAC.

		StD	MAD	POD	FAC
INST.	SEVIRI	26 %	18 %	71 %	29 %
	AVHRR (H.)	22 %	15 %	81 %	19 %
	AVHRR (L.)	28 %	19 %	70 %	30 %
DM	SEVIRI	15 %	12 %	–	–
	AVHRR (H.)	14 %	12 %	–	–
	AVHRR (L.)	15 %	12 %	–	–

AMTD
6, 11145–11179, 2013

Table 2. Table of all results of the validation of the INST and DM SEVIRI data in Hannover, Germany. The data has been compared to SYNOP and HSI and the results are presented as StD, MAD, POD and FAC.

		StD	Bias	POD	FAC
INST.	SYNOP	41 %	51 %	44 %	56 %
	HSI	25 %	21 %	71 %	29 %
DM	SYNOP	31 %	25 %	–	–
	HSI	15 %	19 %	–	–

AMTD
6, 11145–11179, 2013

Table 3. Standard deviations of the differences (StD) and MAD in % DM CFC between HSI and SEVIRI as a function of different Cloud Contamination Factors (50 %, 75 % and 10 %) and grid sizes (3 × 3, 5 × 5 and 7 × 7) in Hannover, Germany from 1 July 2009 to 30 September 2009.

Grid Size	CCF	StD	MAD
3 × 3	50 %	14 %	18 %
	75 %	14 %	14 %
	100 %	15 %	12 %
5 × 5	50 %	15 %	19 %
	75 %	14 %	14 %
	100 %	15 %	12 %
7 × 7	50 %	15 %	17 %
	75 %	14 %	14 %
	100 %	15 %	12 %

AMTD
6, 11145–11179, 2013

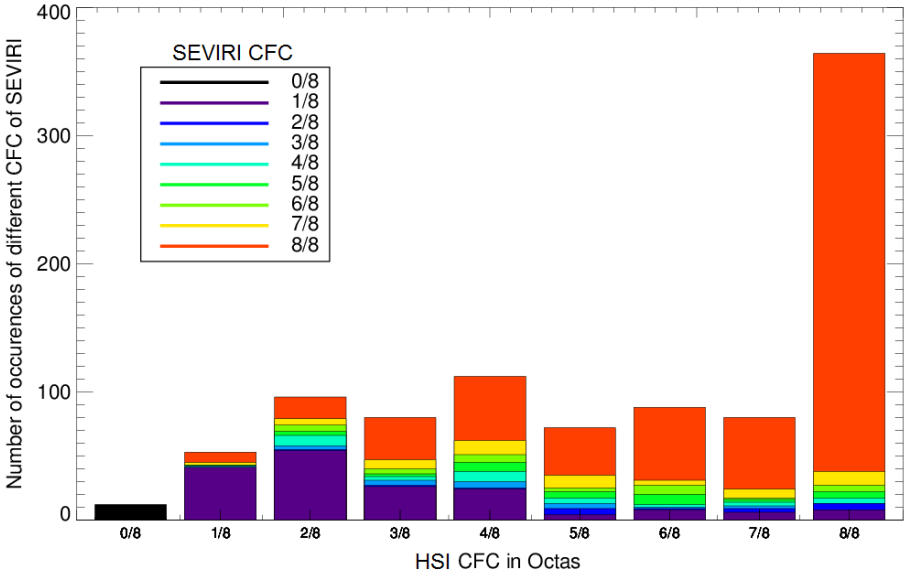

Fig. 1. Histogram of the occurrences of the CFC by SEVIRI as a function of INST CFC in octas by HSI. Each color of one bar represents the CFC by SEVIRI for one of the nine possible values in octas. These are the results from 1 July 2009 to 30 September 2009 for Hannover. Only cloudless sky is detected accurately by both algorithms, but in many cases the SEVIRI algorithm detects full coverage whereas the cloud camera shows lower coverage.

AMTD
6, 11145–11179, 2013

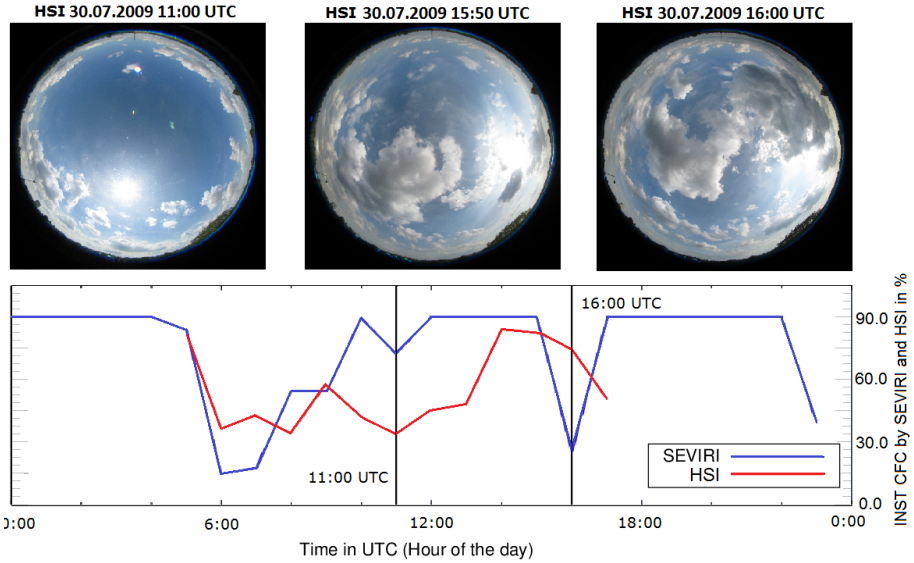

Fig. 2. INST CFC by SEVIRI (blue) and ACS (red) for 30 July 2009 in Hannover-Herrenhausen. The deviations vary between approximately 0 % and 50 % during the day. The MAD is 36 % and the StD is 26 %. These deviations are due to high wind speeds and rapidly changing CFCs.

AMTD
6, 11145–11179, 2013

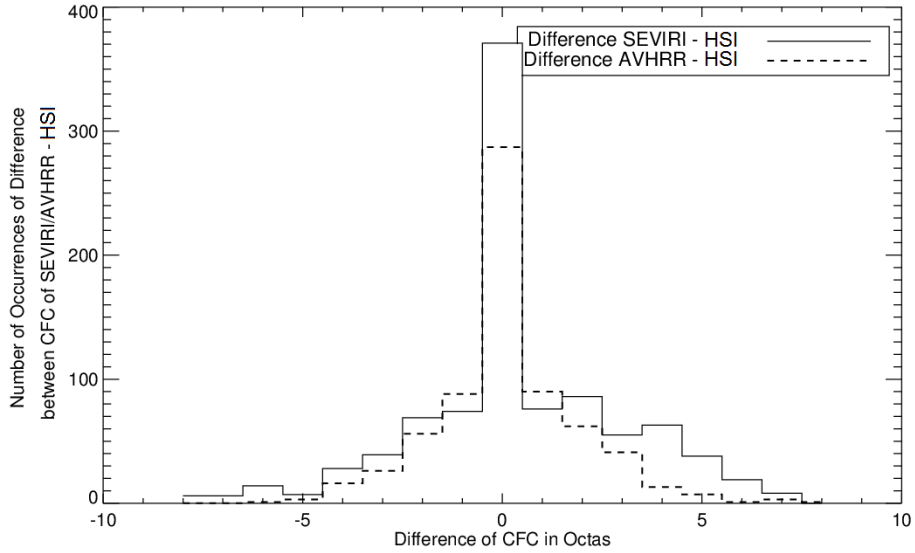

Fig. 3. Number of occurrences of the instantaneous differences (solid line: SEVIRI minus HSI; dashed line: AVHRR minus HSI) in octas in Hannover from 1 July 2009 to 30 September 2009. The negative differences express a higher estimation of the CFC by the HSI compared to the satellite instruments; positive difference expresses a lower estimation respectively. In both cases the highest number of occurrences corresponds to a 0 octa difference, so in the moment where in both cases the estimations coincide.

AMTD
6, 11145–11179, 2013

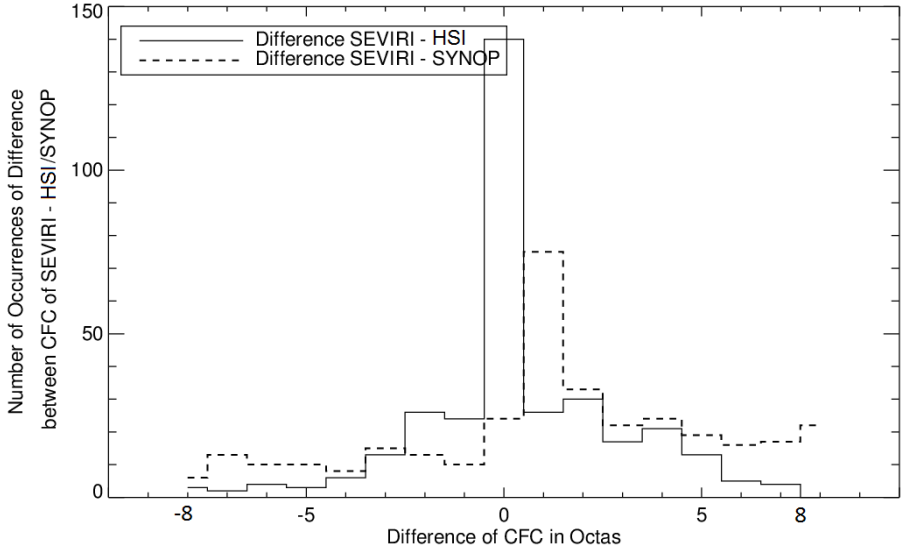

Fig. 4. Histogram of instantaneous CFC differences (solid line: SEVIRI minus HSI in Hannover-Herrenhausen; dashed line: SEVIRI minus SYNOP in Hannover-Langenhagen (SYNOP)) on 1 July 2009 to 30 September 2009. The chosen data points in this figure correspond to the availability of SYNOP data (3-hourly). Negative (positive) differences indicate that SEVIRI underestimates (overestimates) CFC compared to the respective reference (HSI or SYNOP). The CFC difference between SEVIRI and HSI has the highest frequency when both estimations coincide, whereas the peak of the difference between HSI and SYNOP is at one octa.

AMTD
6, 11145–11179, 2013

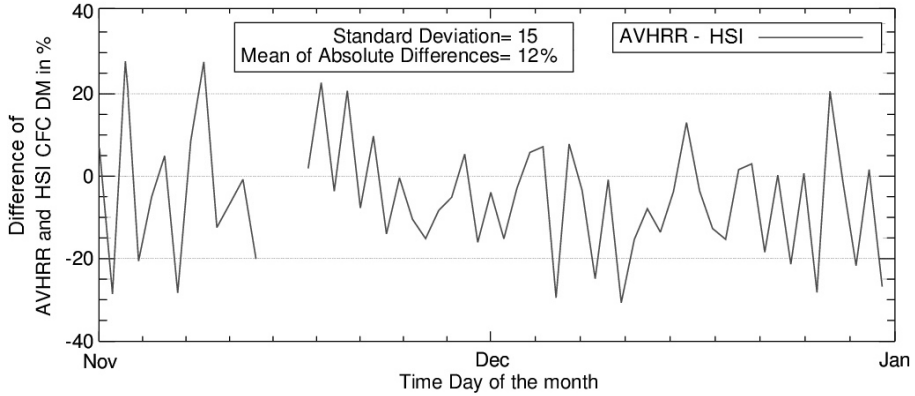

Fig. 5. Differences between DM AVHRR and HSI CFC in % in Lauder, New Zealand between 1 November 2009 and 31 December 2009. The graph shows the largest differences on 2 and 3 November 2009, when AVHRR first estimates a CFC that is almost 30 % lower than estimated by HSI, and on the following day a 30 % higher CFC.

AMTD
6, 11145–11179, 2013